Age-Dependent Retinal Iron Accumulation and Degeneration in Hepcidin Knockout Mice

Majda Hadziahmetovic,[1] *Ying Song,*[1] *Padmavathi Ponnuru,*[2] *Jared Iacovelli,*[1] *Allan Hunter,*[1] *Nadine Haddad,*[1] *John Beard,*[3,4] *James R. Connor,*[2] *Sophie Vaulont,*[5,6] *and Joshua L. Dunaief*[1]

Purpose. Iron dysregulation can cause retinal disease, yet retinal iron regulatory mechanisms are incompletely understood. The peptide hormone hepcidin (Hepc) limits iron uptake from the intestine by triggering degradation of the iron transporter ferroportin (Fpn). Given that Hepc is expressed in the retina and Fpn is expressed in cells constituting the blood-retinal barrier, the authors tested whether the retina may produce Hepc to limit retinal iron import.

Methods. Retinas of Hepc$^{-/-}$ mice were analyzed by histology, autofluorescence spectral analysis, atomic absorption spectrophotometry, Perls' iron stain, and immunofluorescence to assess iron-handling proteins. Retinal Hepc mRNA was evaluated through qPCR after intravitreal iron injection. Mechanisms of retinal Hepc upregulation were tested by Western blot analysis. A retinal capillary endothelial cell culture system was used to assess the effect of exogenous Hepc on Fpn.

Results. Hepc$^{-/-}$ mice experienced age-dependent increases in retinal iron followed by retinal degeneration with autofluorescent RPE, photoreceptor death, and subretinal neovascularization. Hepc$^{-/-}$ mice had increased Fpn immunoreactivity in vascular endothelial cells. Conversely, in cultured retinal capillary endothelial cells, exogenous Hepc decreased both Fpn levels and iron transport. The retina can sense increased iron levels, upregulating Hepc after phosphorylation of extracellular signal regulated kinases.

Conclusions. These findings indicate that Hepc is essential for retinal iron regulation. In the absence of Hepc, retinal degeneration occurs. Increases in Hepc mRNA levels after intravitreal iron injection combined with Hepc-mediated decreases in iron export from cultured retinal capillary endothelial cells suggest that the retina may use Hepc for its tissue-specific iron regulation. (*Invest Ophthalmol Vis Sci.* 2011;52:109–118) DOI:10.1167/iovs.10-6113

Although iron is an essential cofactor in numerous basic metabolic processes, the increase in iron levels that occurs with aging in many tissues[1] may exacerbate age-related diseases through iron-induced oxidative stress.[2–6] Iron overload has been implicated in age-related neurodegenerative diseases affecting the brain (including Parkinson's[7,8] and Alzheimer's diseases[9]) and affecting the retina (age-related macular degeneration [AMD]). In AMD, iron accumulates in photoreceptors, RPE, and Bruch's membrane.[10]

Hereditary iron overload is also associated with neurodegeneration. CNS iron accumulation is thought to promote neurodegeneration in Friedreich's ataxia, pantothenate kinase–associated neurodegeneration, neuroferritinopathy, and aceruloplasminemia. Patients with the latter have early-onset macular degeneration associated with elevated retinal iron levels.[11–13] These findings, together with the iron accumulation in AMD retinas, suggest that, in addition to the previously described influences of inflammation and the complement cascade,[14–16] disturbed iron metabolism may play a role in the pathogenesis of AMD. Increased understanding of iron regulation in the retina and the CNS in general is important.

Separation of the neural retina from its blood supply combined with the potential toxicity of excess iron suggests the need for intercellular signaling to regulate iron flux across the blood-retinal barrier. A potential mediator of such intercellular signaling within the retina is suggested by recent studies of systemic iron regulation. At the systemic level, the peptide hormone hepcidin (Hepc) serves as a master regulator of iron homeostasis.[17] Hepc is predominantly synthesized in the liver[18] and is secreted into the bloodstream. Circulating Hepc triggers internalization and degradation of the iron exporter ferroportin (Fpn) in macrophages and in enterocytes, preventing iron export from these cells.[19] Hepc synthesis is induced by inflammation, infection, and iron.[20,21] Conversely, Hepc expression is diminished in response to hypoxia and anemia.[22] The importance of Hepc in iron metabolism was confirmed in two mouse models. *Hepc1*$^{-/-}$ mice demonstrated multivisceral iron overload.[23] Conversely, mice that overexpress *Hepc1* were born with severe iron deficiency that was incompatible with life.[24] Herein, we refer to the protein product of the *Hepc1* gene as Hepc.

Hepc expression was found in the retina within photoreceptors, Müller cells, and RPE,[25] suggesting that the retina may produce Hepc for the regulation of local iron homeostasis. To assess the importance of Hepc for retinal iron regulation and health, we studied iron levels and retinal morphology in *Hepc1*$^{-/-}$ mice of several ages, tested the effects of elevated retinal iron levels on *Hepc* mRNA levels, and, in a tissue culture model of the blood-retinal barrier, tested the influence of exogenous Hepc on Fpn levels and iron transport.

From the [1]F. M. Kirby Center for Molecular Ophthalmology, Scheie Eye Institute, University of Pennsylvania, Philadelphia, Pennsylvania; [2]Department of Neurosurgery, Pennsylvania State Hershey Medical Center, Hershey, Pennsylvania; [3]Department of Nutrition, College of Health and Human Development, Pennsylvania State University, University Park, Pennsylvania; [5]Institut Cochin, Université Paris Descartes, CNRS (UMR 8104), Paris, France; and [6]Inserm, U567, Paris, France.

[4]Deceased, February 13, 2009.

Supported by National Institutes of Health Grant EY015240-05A1S1, the International Retina Research Foundation, American Health Assistance Foundation, and Agence Nationale de la Recherche.

Submitted for publication June 24, 2010; revised July 20, 2010; accepted July 26, 2010.

Disclosure: **M. Hadziahmetovic**, None; **Y. Song**, None; **P. Ponnuru**, None; **J. Iacovelli**, None; **A. Hunter**, None; **N. Haddad**, None; **J. Beard**, None; **J.R. Connor**, None; **S. Vaulont**, None; **J.L. Dunaief**, None

Corresponding author: Joshua L. Dunaief, 305 Stellar Chance Labs, 422 Curie Boulevard, Philadelphia, PA 19104; jdunaief@upenn.edu.

Materials and Methods

Animals

Hepc1 knockout mice (*Hepc1*$^{-/-}$) on a C57BL/6 background were generated as previously described.[23] C57BL/6 wild-type (WT) mice, C57BL/6 mice with a targeted mutation in the *Cp* gene (Cp$^{-/-}$), and natural mutation in the *Heph* gene (*Heph*$^{sla/sla}$ or *Heph*$^{sla/Y}$) were generated as previously described[26] and are referred to herein as *Cp/Heph* double-knockout (DKO) (*Cp/Heph* DKO). *IL6*$^{-/-}$ mice (B6.129S2-*IL6*^{tm1Kopf}/J) were obtained from The Jackson Laboratory (Bar Harbor, ME). All procedures were approved by the European convention for the protection of laboratory animals and the Institutional Animal Care and Use Committee of the University of Pennsylvania and complied with the ARVO Statement for the Use of Animals in Ophthalmic and Vision Research. Eyes were enucleated immediately after death and were fixed overnight either in 2% paraformaldehyde and 2% glutaraldehyde for histochemical iron detection and morphologic analysis or in 4% paraformaldehyde for immunofluorescence.

Histochemical Iron Detection by Perls' Staining and Morphologic Analysis

After several days of fixation in 2% paraformaldehyde and 2% glutaraldehyde, eyecups were made by removing the anterior segment. The tissues were then dehydrated in ethanol and infiltrated overnight in embedding solution (JB4 Solution A; Polysciences, Inc., Warrington, PA). The next day, the eyecups were embedded in plastic (JB4; Polysciences, Inc). Then 3-μm-thick plastic sections were stained with either Perls' for histochemical iron detection as previously described[27] or toluidine blue for standard histology.[27] Stained sections were observed and photographed with a microscope (TE-300; Nikon, Tokyo, Japan).

Spectral Analysis of Tissue Autofluorescence

Cryosections measuring 10 μm were mounted with fluorescence mounting media (KPL) and coverslipped. Sample autofluorescence was excited with the 488-nm argon laser of a confocal microscope (LSM-510; Carl Zeiss, Oberkochen, Germany) running in Lambda scan mode, and emission spectra were acquired from 500 nm to 714 nm. Data analysis was performed using version 4.0 of the LSM image browser.

Quantitative Iron Detection

Eyes from *Hepc1*$^{-/-}$ and age-matched *Hepc1*$^{+/+}$ mice were fixed in 4% paraformaldehyde. Eyecups were made by removing the anterior segment. The ciliary body was removed with a curved scalpel blade, and the neurosensory retina was detached from the underlying RPE/choroid tissue. Samples of the neurosensory retina and RPE/choroids (with sclera) were placed in separate tubes and allowed to dry at room temperature. For quantification of total iron in these tissues, graphite furnace atomic absorption spectrophotometry (model 5100AA; Perkin Elmer, Boston, MA) was performed as we have described.[26]

Immunofluorescence

Globes fixed in 4% paraformaldehyde were rinsed in PBS, and the eyecups were dissected. Eyecups were cryoprotected in 30% sucrose overnight, then embedded in optimal cutting temperature compound (OCT; Tissue-Tek, Sakura Finetek, Torrance, CA). Immunofluorescence was performed on 10-μm-thick sections, as previously described.[28] Primary antibodies were rabbit anti–light ferritin (F17) at 1:2500 dilution (generous gift of Paolo Santambrogio and Paolo Arosio, Instituto di Ricovero e Cura a Carattere Scientifico, Milan, and Universiti of Brescia, Brescia, Italy respectively), rabbit anti-Fpn at 1: 80 dilution (Orbigen, San Diego, CA), mouse anti-CD31 at 1 to 100 dilution (BD Biosciences, San Jose, CA), or rabbit anti-RPE65 at 1 to 400 dilution (generous gift of Michael Redmond, National Eye Institute, Bethesda, MD). Primary antibody reactivity was detected using fluorophore-labeled secondary antibodies (Jackson ImmunoResearch Laboratories, West Grove, PA). Control sections were treated identically but with omission of the primary antibody. Sections were analyzed by fluorescence microscopy with identical exposure parameters using the microscope (TE300; Nikon) with ImagePro software, and quantification of immunoreactivity was performed by measuring the mean pixel intensity within the RPE and neural retina of each photomicrograph.

Quantitative Real-Time PCR

Neurosensory retina and RPE/choroid samples obtained from *Hepc1*$^{-/-}$, *IL6*$^{-/-}$, *Cp/Heph* DKO, and WT mice were analyzed using quantitative RT-PCR for gene expression. RNA isolation was performed with a mini kit (RNeasy Mini Kit; Qiagen, Valencia, CA) according to the manufacturer's protocol. RNA was quantified with a spectrophotometer and stored at −80°C. cDNA was synthesized with reverse transcription reagents (TaqMan; Applied Biosystems, Darmstadt, Germany) according to the manufacturer's protocol. Gene expression assays (TaqMan; Applied Biosystems) were obtained and used for PCR analysis. Probes used were transferrin receptor (*Tfrc*, Mm00441941_m1), hepcidin antimicrobial peptide (*Hamp1*, Mm00519025_m1), solute carrier family 40 (*Slc40a1*, Mm00489837_m1), interleukin 6 (*IL6*, Mm00446190_m1), bone morphogenetic protein 6 (*BMP6*, Mm 00432095_m1), and complement component factor H (*Cfh*, Mm00438186_m1). Eukaryotic 18S rRNA (Hs99999901_s1) served as an internal control because of its constant expression level across the studied sample sets. Real-time RT-PCR (TaqMan; Applied Biosystems) was performed (ABI Prism 7500 Sequence Detection System; Applied Biosystems) using the $\Delta\Delta C_T$ method, which provides normalized expression values. The amount of target mRNA was compared among the groups of interest. All reactions were performed in biological (three mice) and technical (three qPCR replicates per mouse) triplicates.

Needle Injury and Intravitreal Injections

Needle injury was performed with a 30-gauge needle in the superior temporal region of the eye. Ten penetrations were made, and the retinas were collected 6 hours after trauma. Intravitreal injections were delivered through 32-gauge needles connected to 10-μL microsyringes (Hamilton, Reno, NV). The right eye of each animal was injected with 2 μL of 1.2 mM holo-transferrin (Holo-Tf), and the left eye was injected with 2 μL of 1.2 mM Apo-Tf as control (Millipore, Billerica, MA). Mice were euthanized at the indicated time points after the injections, and the retinas were collected.

Western Blot Analysis

After intravitreal injection of Holo-Tf and Apo-Tf, mice were killed at the indicated time points. Then neurosensory retinas were dissected and processed for Western blot analysis. Briefly, after homogenization, retinas were lysed in RIPA buffer, and protein was quantified (BCA Protein Assay Kit; Thermo Scientific, Rockford, IL). Thirty micrograms of total protein was used in each lane. Samples were incubated for 10 minutes at 70°C. Protein lysates were separated on 4% to 12% SDS-PAGE and transferred to nitrocellulose membrane. Blocking was achieved by incubation in Tris-buffered saline containing 5% milk and 0.1% Tween 20. Membranes were incubated overnight at 4°C with rabbit anti–phospho-Smad1(Ser463/465)/Smad5(Ser464/465)/Smad8(Ser426/428) antibody at 1:1000 dilution, rabbit anti–Smad5 antibody at 1:1000, rabbit anti–phospho-p44/42 MAPK (Erk1/2) (Thr202/Tyr204) antibody at 1:5000, and mouse anti–p44/42 MAPK antibody at 1:5000 (Cell Signaling Technology, Beverly MA). After washes, membranes were incubated with donkey anti–rabbit-horseradish peroxidase (HRP) at a 1:10,000 dilution (GE Healthcare, Little Chalfont, Buckinghamshire, UK) and were developed using reagent (ECL Plus; GE Healthcare). Images were acquired (Typhoon 9400 Variable Mode Imager; GE Healthcare), and densitometry was performed (ImageQuant TL; GE Healthcare).

In Vitro Experiments on Bovine Retinal Endothelial Cells

Bovine retinal endothelial cells (BRECs) were grown in media (MCDB 131; Gibco, Rockville, MD) supplemented with 10% FBS (Gemini, 10 ng/mL EGF; (Invitrogen, Carlsbad, CA), 0.2 mg/mL endothelial cell growth factor (ENDO GRO; VEC Technologies, Inc., Rensselaer, NY), 0.09 mg/mL heparin (Fisher Scientific, Fair Lawn, NJ), and antibiotic/antimycotic (Gibco, Rockville, MD). For the experiments, BRECs were gently trypsinized and grown to confluence on the porous filters (0.4 μm pore size) of the inserts (Transwell; Corning Life Sciences, Wilkes Barre, PA) coated with fibronectin (Sigma, St. Louis, MO). Serum-free and EGF-free medium was then added to the BRECs with 138 nm hydrocortisone (Sigma) for 48 hours. ^{59}Fe-nitrilotriacetate (NTA) complex was prepared with 200 μL of 1 mM NTA, 2.8 μL of ferrous ammonium sulfate (from 1 mg/mL stock), 20 μL diluted $^{59}FeCl_3$ (2-fold in dH_2O; Perkin Elmer, Waltham, MA), and 10 μL of 0.5 M sodium bicarbonate. This complex was added to the upper chamber of the insert (Transwell; Sigma) and was incubated overnight at 37°C. The cells were rinsed twice with PBS the following morning and were placed in serum-free, EGF-free medium (MCDB 131; Gibco) with or without hepcidin (700 nm; Peptide Institute, Inc., Osaka, Japan) in the basal chamber. RITC-dextran (Sigma) was included in the media in the upper chamber to ensure the integrity of the intercellular junctions in this model. The fluorescence of the aliquots from the lower chamber was read at 555 to 585 nM, (570 nM cutoff) in a fluorescence plate reader (Spectra Max Gemini; Molecular Devices, Sunnyvale, CA). ^{59}Fe transport into the lower chamber was measured by removal of an aliquot 1 hour after iron loading was complete. After 1 hour, no further increase in basal chamber ^{59}Fe occurred, suggesting rapid saturation of the medium.

To analyze the expression of ferroportin, BRECs were seeded in six-well plates—three wells for each condition—and were incubated overnight. The next morning, BRECs were rinsed twice with PBS and placed in serum-free and EGF-free medium (MCDB 131; Gibco) for 1 hour with or without Hepc (700 nm). Then the cells were rinsed with PBS and harvested, and cell lysates were prepared using RIPA buffer (Sigma). After sonication for 30 seconds on ice, the lysates were centrifuged at 10,000 rpm, and supernatant was collected. Thirty micrograms of total protein was loaded for each sample on 4% to 20% gradient SDS-PAGE gels (Bio-Rad, Hercules, CA) and was transferred to nitrocellulose membrane (Pall Corporation, Pensacola, FL) for 1 hour at 100 V. The membrane was blocked for 1 hour in 5% nonfat milk at room temperature and was incubated with anti-Fpn (rabbit polyclonal; Alpha Diagnostics, San Antonio, TX) diluted at 1:1000 overnight at 4°C. After washes, the membrane was incubated with anti-rabbit HRP-conjugated secondary antibody (GE Healthcare; 1:5000 dilution) for 1 hour at room temperature. Enhanced chemiluminescence was performed for 1 minute, and the membrane was scanned using a Fujifilm (Valhalla, NY) system.

Statistical Analysis

Mean ± SE was calculated for each comparison group. Means between the groups were compared using the two-group *t*-test. $P < 0.05$ was considered statistically significant. Results are presented as mean ± SEM. All analyses were performed with statistical software (GraphPad Software, Inc. San Diego, CA).

Results

Retinal Degeneration in 18-Month-Old *Hepc1*$^{-/-}$ Mice

Retinas from *Hepc1*$^{-/-}$ mice were normal at 3 months ($n = 3$; data not shown), had mild, focal abnormalities at 9 months ($n = 3$), and showed severe changes at 18 months ($n = 3$). Nine-month-old *Hepc1*$^{-/-}$ retinas had focal areas of retinal pigment epithelial cell hyperplasia (involving <5% of total retina), with loss of photoreceptor outer segments and subretinal neovascularization (Fig. 1B). At 18 months, approximately 10% of the total retina had massively hypertrophic retinal pigment epithelial cells accompanied by local loss of photoreceptor inner and outer segments and thinning of the photore-

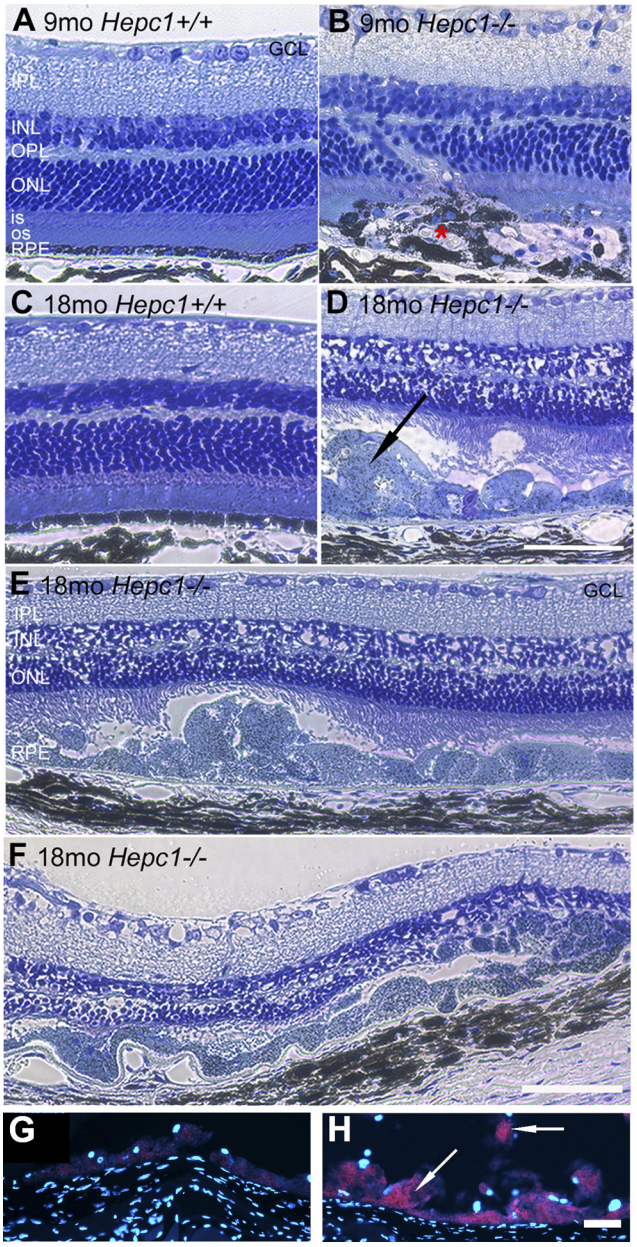

Figure 1. *Hepc*$^{-/-}$ mice have retinal degeneration. Bright-field micrographs of plastic sections show that compared with 9-month-old *Hepc*$^{+/+}$ mice (**A**), the age-matched *Hepc*$^{-/-}$ mice had focal areas of retinal pigment epithelial hyperplasia (**B**) and subretinal neovascularization (**B**, *red asterisk*). Compared with 18-month-old control (**C**), 18-month-old *Hepc*$^{-/-}$ mice (**D**–**F**) had focal areas of massively hypertrophic retinal pigment epithelial cells (**D**, *arrow*), with degeneration of overlying photoreceptor inner and outer segments and thinning of the outer and inner nuclear layers. Photomicrographs of 18-month-old *Hepc*$^{-/-}$ mice show strong RPE65 immunoreactivity within the hypertrophic retinal pigment epithelial cells (**H**, *arrows*) compared with no primary antibody (**G**) negative control. Scale bars: 25 μm (**A**–**D**, **G**, **H**); 50 μm (**E**, **F**). OS, photoreceptor outer segment; IS, photoreceptor inner segment; ONL, outer nuclear layer; OPL, outer plexiform layer; INL, inner nuclear layer; IPL, inner plexiform layer; GCL, ganglion cell layer.

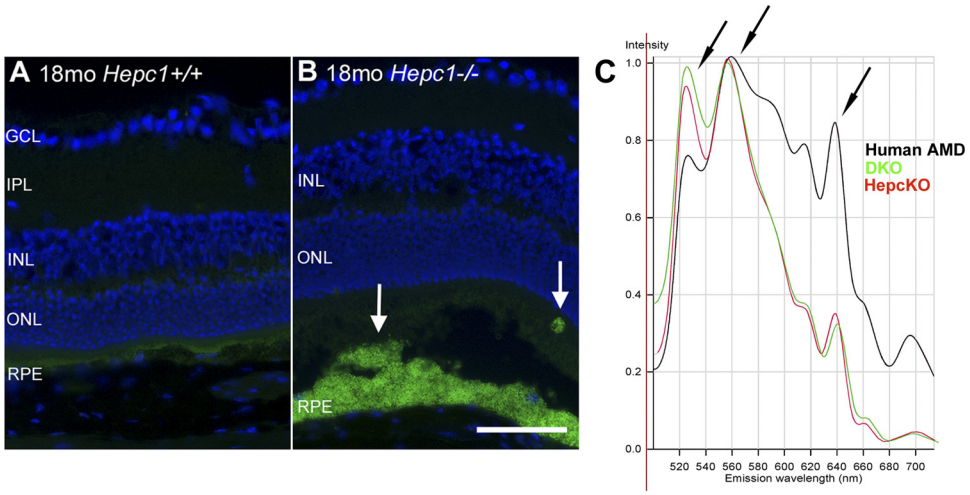

Figure 2. Lipofuscin-like material in *Hepc1*$^{-/-}$ hypertrophic RPE. Fluorescence photomicrographs showing *green* autofluorescent lipofuscin-like material in 18-month-old *Hepc*$^{-/-}$ RPE (**B**, *arrows*), whereas the age-matched controls had only minimal autofluorescence within photoreceptor outer segments and none detected in the RPE. Nuclei are stained with DAPI (*blue*). Spectral analysis of relative autofluorescence emission intensities (with 488 nm excitation) revealed several similar emission peaks (*arrows*) among hypertrophic retinal pigment epithelial cells from *Hepc1*$^{-/-}$ and DKO mice compared with RPE from the post mortem retina of a patient with AMD (**C**). Scale bar, 25 μm. OS, photoreceptor outer segment; IS, photoreceptor inner segment; ONL, outer nuclear layer; OPL, outer plexiform layer; INL, inner nuclear layer; IPL, inner plexiform layer; GCL, ganglion cell layer.

ceptor outer nuclear layer (Figs. 1D-F). Comparisons were made to age, sex, and strain-matched *Hepc1*$^{+/+}$ retinas in which the morphology was normal (Figs. 1A, 1C; $n = 3$). To confirm the identity of the hypertrophic cells found in 18-month-old *Hepc1* $^{-/-}$ mice, anti–RPE65 immunolabeling was performed. Strong RPE65 immunoreactivity was detected within the cells (Fig. 1H). Electroretinography in 9-month-old *Hepc1*$^{-/-}$ mice revealed no reduction in the summated response of the whole retina to light (not shown) because the retinal degeneration was focal.

Lipofuscin-like Material in Hypertrophic Retinal Pigment Epithelial Cells of *Hepc1*$^{-/-}$ Mice

Autofluorescent lipofuscin builds up within the RPE during aging and can act as a photosensitizer.[29] A number of studies suggest it may be toxic to the RPE and may contribute to AMD pathogenesis.[30] In contrast to minimal fluorescence in retinas of 18-month-old *Hepc1*$^{+/+}$ mice (Fig. 2A; $n = 3$), bright autofluorescence was detected by fluorescence microscopy in the hypertrophic RPE of 18-month-old *Hepc1*$^{-/-}$ mice (Fig. 2B; $n = 3$). Spectral analysis of autofluorescent, hypertrophic retinal pigment epithelial cells from *Hepc1*$^{-/-}$ mice compared with retinal pigment epithelial cells in the post mortem eye of a patient with AMD revealed several similar emission peaks (Fig. 2C), suggesting that some of the lipofuscin components were similar. Nearly identical spectral emission results were obtained in retinal pigment epithelial cells from *Hepc1*$^{-/-}$ mice and *Cp/Heph* DKO mice (Fig. 2C), which also experience age-dependent retinal pigment epithelial iron accumulation with retinal degeneration.[26,27] These results suggest that iron-induced oxidation causes accumulation of similar autofluorescent molecules in both mouse strains. The development of autofluorescence in both the *Hepc1*$^{-/-}$ mice and the *Cp/Heph* DKO RPE is age dependent, first observed at 12 months in *Hepc1*$^{-/-}$ mice (not shown), and is most prominent in hypertrophic retinal pigment epithelial cells.

Localization and Quantification of Iron in the Retina and Ciliary Body of *Hepc1*$^{+/+}$ and Age-Matched *Hepc1*$^{-/-}$ Mice

Neural retinas of 12.5-month-old *Hepc1*$^{-/-}$ mice ($n = 4$) had fivefold higher iron levels measured by atomic absorption spectrophotometry (Fig. 3A) compared with age-matched controls (*Hepc1*$^{+/+}$; $P < 0.01$; $n = 4$). The RPE/choroids in these mice also had significantly higher (threefold; $P < 0.01$; $n = 4$) iron levels than the age-matched control group (Fig. 3B; $n = 4$). Iron quantification results were consistent with histochemical iron detection by which strong granular Perls' stain (Figs. 3C3, 3C4) was present in the RPE of 18-month-old *Hepc1*$^{-/-}$ mice ($n = 3$), whereas none was detected in age-matched WT mice (Figs. 3C1, 3C2; $n = 3$). The ciliary body of 18-month-old *Hepc1*$^{-/-}$ mice also had strong Perls' label, primarily in the nonpigmented ciliary epithelium (Fig. 3C4; $n = 3$), whereas the ciliary body of an age-matched WT mouse did not have any visible iron accumulation (Fig. 3C2; $n = 3$). Three- and 9-month-old *Hepc1*$^{-/-}$ mouse eyes had no detectable Perls' signal (data not shown).

Hepc1$^{-/-}$ Eyes Had Increased L-Ferritin Protein and Decreased *Tfrc mRNA*

The levels of the cytosolic iron storage protein ferritin and the *Tfrc* mRNA are regulated in opposite directions by cytosolic labile iron levels. This is accomplished through iron regulatory proteins IRP1 and IRP2[31–33] so that when labile iron levels are high, ferritin translation increases while *Tfrc* mRNA stability decreases. Consistent with the elevated iron levels detected in *Hepc1*$^{-/-}$ mice by atomic absorption spectrophotometry and Perls' staining, levels of L-ferritin protein increased and *Tfrc* mRNA decreased. L-ferritin immunoreactivity was increased in *Hepc1*$^{-/-}$ mice at sites of iron accumulation detected by atomic absorption and Perls' staining. Ferritin increased with age in 3-, 9-, and 18-month-old *Hepc1*$^{-/-}$ mice (Figs. 4B, 4D, 4F; $n = 3$ each age group) compared with the age-matched *Hepc1*$^{+/+}$ mice (Figs. 4A, 4C, 4E; $n = 3$ each age group). In *Hepc1*$^{-/-}$ mice, L-ferritin was present in bipolar cell

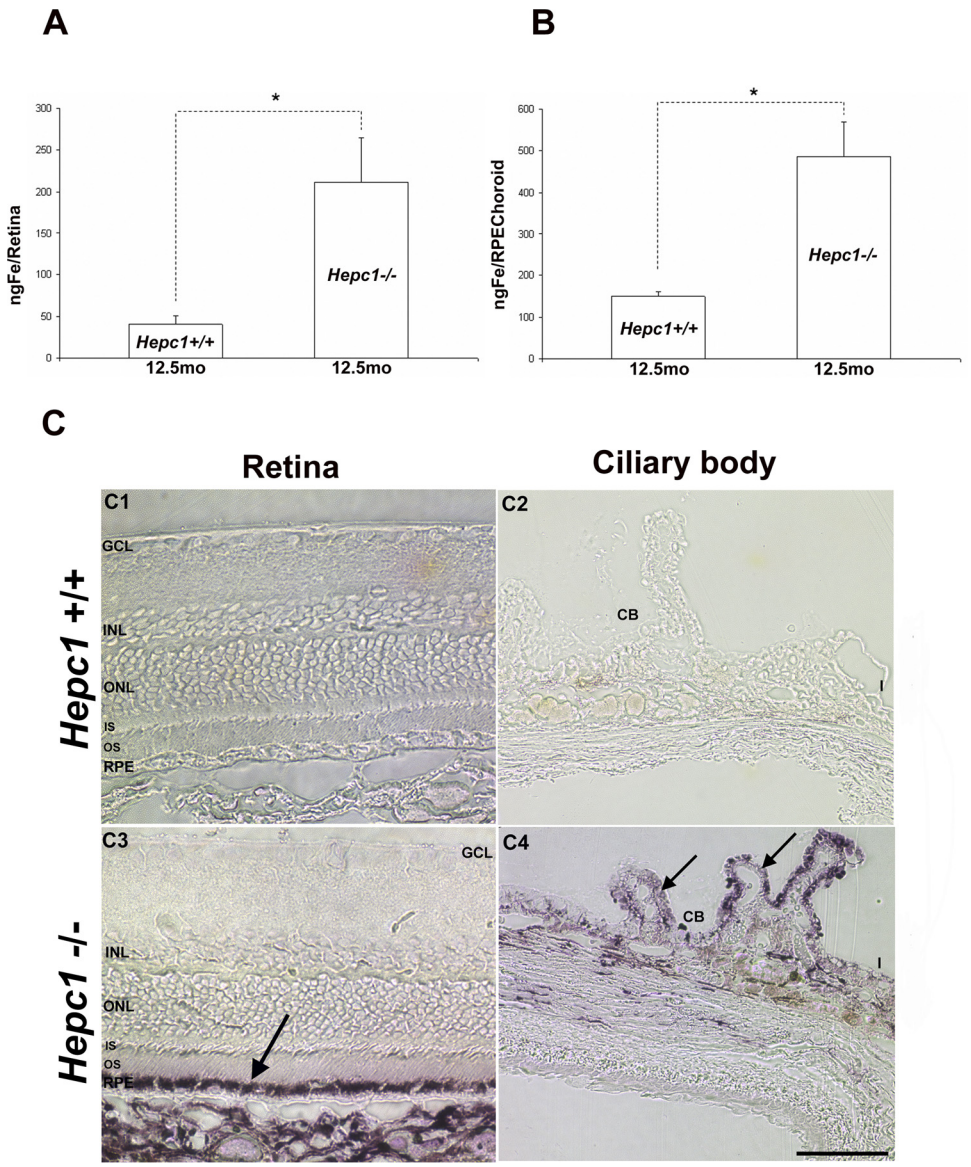

FIGURE 3. Quantification and histochemical detection of iron in $Hepc^{+/+}$ and age-matched $Hepc^{-/-}$ mice. Graphs of iron in the retinas and RPE/choroid of 12.5-month-old $Hepc^{-/-}$ *and* $Hepc^{+/+}$ (control) mice measured by atomic absorption spectrophotometry. Total iron in nanograms per neurosensory retina (**A**) and in nanograms per RPE/choroid (**B**) is shown for two different genotypes. *Significant difference ($P < 0.05$). Bright-field photomicrographs of Perls'-stained plastic-embedded $Hepc^{+/+}$ (**C1**, **C2**) and $Hepc^{-/-}$ (**C3**, **C4**) retinas (**C1**, **C3**) and ciliary bodies (**C2**, **C4**) demonstrated iron accumulation in the RPE (**C3**, *arrow*) and choroid of 18-month-old $Hepc^{-/-}$ mice. Iron also accumulated in the nonpigmented ciliary epithelium in 18-month-old $Hepc^{-/-}$ (**C4**, *arrows*). Controls ($Hepc^{+/+}$) did not have Perls' signal in either the RPE or the ciliary body (**C1**, **C2**). Scale bar, 50 μm.

axon termini in the inner plexiform layer and in the outer plexiform layer, RPE, and choroid. The levels of L-ferritin were also increased in the ciliary body of 3-, 9-, and 18-month-old $Hepc1^{-/-}$ mice (Figs. 4B′, 4D′, 4F′) compared with the age-matched controls (Figs. 4A′, 4C′, 4E′). Immunoreactivity was strongest in nonpigmented ciliary epithelium and increased in intensity with age.

TfRc mRNA levels decreased in RPE/choroid of the $Hepc1^{-/-}$ mice by 2.4-fold (Fig. 4G; $n = 3$) compared with age-matched WT mice, consistent with the IRP-regulated mechanism preventing the iron-overloaded cells from accumulating more iron. In neural retina, *TfRc* was downregulated by 1.4-fold (Fig. 4H; $n = 3$).

Levels of Fpn Protein Were Increased in $Hepc1^{-/-}$ Retinas

Levels of the transmembrane iron exporter Fpn are controlled by Hepc-mediated internalization and degradation. Thus, $Hepc1^{-/-}$ mice might be expected to have elevated Fpn protein levels because of the lack of Hepc-mediated Fpn protein degradation. Comparing $Hepc1^{+/+}$ and $Hepc1^{-/-}$ retinas ($n = 3$ each), Fpn immunoreactivity was strongly increased in vascular endothelial cells (Figs. 5B, 5D, 5F, arrows) of $Hepc1^{-/-}$ mice compared with age-matched controls. Colabeling with endothelial marker CD-31 suggested Fpn localization on the abluminal side of the vascular endothelium (Figs. 5E, 5F arrows). Fpn immunoreactivity was moderately increased throughout the retinas of $Hepc1^{-/-}$ mice compared with age-matched WT controls (Fig. 5G pixel density graph; $n = 3$). Elevated levels of retinal Fpn were also detected when retinal sections were immunolabeled with a noncommercially produced anti-Fpn antibody (not shown; gift of Jerry Kaplan, Ivana DeDomenico, and Diane Ward, University of Utah).

Hepc Decreased Fpn Levels in Cultured BRECs and Decreased Iron Export from These Cells

Given that $Hepc1^{-/-}$ mice have increased Fpn in retinal vascular endothelial cells, a potential mechanism of retinal iron overload in $Hepc1^{-/-}$ mice is unchecked iron import across the blood-retinal barrier. To test this hypothesis, the effects of physiologic levels of exogenous Hepc peptide were tested in an established retinal capillary endothelial cell culture system. We have previously shown that BRECs grown as a monolayer on transwell filters establish tight junctions and can be used in transepithelial transport assays.[34] BRECs express Fpn, and Fpn

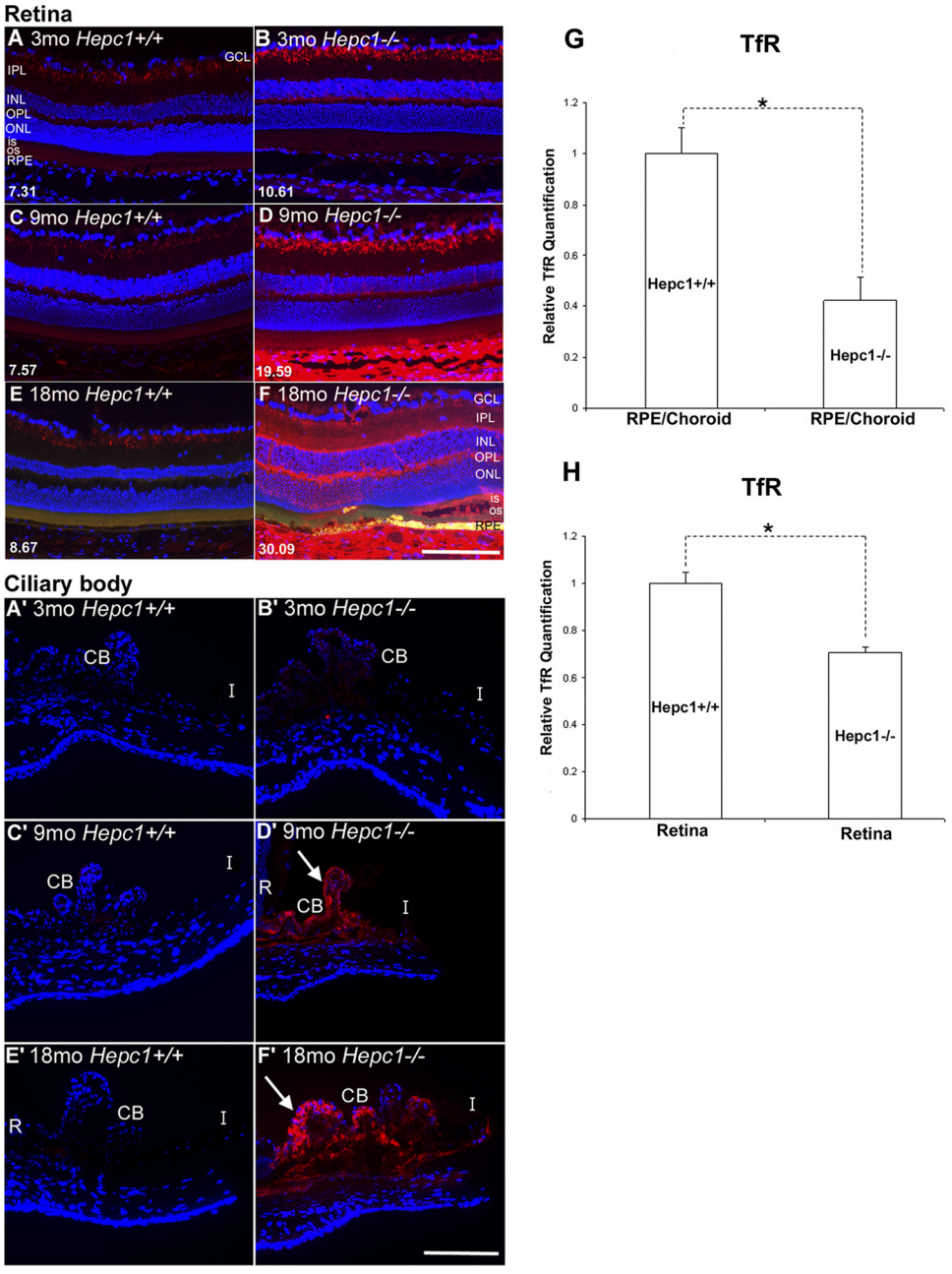

FIGURE 4. *Hepc*$^{-/-}$ retinas and ciliary bodies have increased L-ferritin, and retinas have decreased transferrin receptor mRNA. Fluorescence photomicrographs of 3-, 9-, and 18-month-old *Hepc*$^{-/-}$ retinas (**B**, **D**, **F**) showed stronger immunoreactivity (*red*), increasing with age, throughout the inner plexiform layer, outer plexiform layer, RPE, and choroid compared with the age-matched controls (*Hepc*$^{+/+}$; **A**, **C**, **E**). Immunoreactivity was quantified by measuring the mean pixel intensity within the RPE and neural retina of each photomicrograph (shown in the *lower left corner*). Fluorescence photomicrographs of 3-, 9-, and 18-month-old *Hepc*$^{-/-}$ ciliary bodies (**B′**, **D′**, **F′**) showed strong immunoreactivity mostly within the nonpigmented ciliary epithelium, whereas age-matched controls (**A′**, **C′**, **E′**) had only weak signal. Scale bar, 50 μm. (**G**, **H**) Transferrin receptor mRNA levels in 4-month-old *Hepc*$^{-/-}$ mice compared with the age-matched controls detected by qPCR in RPE/choroids (**G**) and in neural retina (**H**). $^{*}P < 0.05$.

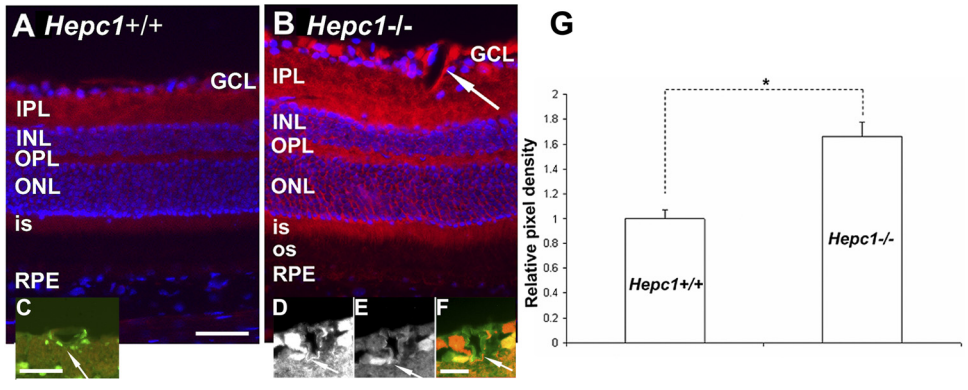

FIGURE 5. *Hepc*$^{-/-}$ mice have increased Fpn protein in the retina. Fluorescence photomicrographs of retinas from *Hepc*$^{-/-}$ mice (4 months old) showing stronger Fpn immunoreactivity (**B**) compared with the age-matched *Hepc*$^{+/+}$ mice (**A**). Fpn immunoreactivity was prominent in the vascular endothelium (**B**, **D**, **F**, *arrows*) of *Hepc*$^{-/-}$ mice but not in vessels from WT mice (**C**). Immunoreactivity was quantified by measuring the mean pixel intensity within the retinal pigment epithelial and neural retinas (**G**; $P < 0.05$). Scale bars: 25 μm (**A**, **B**); 10 μm (**C**); 12.5 μm (**D**–**F**). (**C**) Fpn, *red*; CD-31, *green*. (**D**) Fpn. (**E**) CD31. (**F**) Fpn, *red*; CD31, *green*. OS, photoreceptor outer segment; IS, photoreceptor inner segment; ONL, outer nuclear layer; OPL, outer plexiform layer; INL, inner nuclear layer; IPL, inner plexiform layer; GCL, ganglion cell layer.

protein levels were decreased by exposure to Hepc peptide (Figs. 6A, 6B; $n = 3$). Next, to test whether this Hepc-mediated decrease in Fpn levels affected iron transport, we used radiolabeled iron to assess export in the presence or absence of Hepc. Cells were loaded on the apical side overnight with radiolabeled iron, and then extracellular iron was washed away. Compared with wells with no added Hepc protein, Hepc addition diminished iron export for 1 hour toward the basal (abluminal) side of the cells (Fig. 6C; $n = 3$), analogous to the direction of the neural retina. After 1 hour, no further increase in basal chamber ^{59}Fe occurred, suggesting rapid saturation of the medium by iron (not shown).

Upregulation of *Hepc* in Response to Retinal Iron Overload

To determine whether retina-produced *Hepc1* is regulated by retinal iron, *Hepc1* mRNA levels were measured in retinas from *Cp/Hepb* DKOs, which have an age-dependent increase in retinal pigment epithelium and neural retina iron,[26,27] presumably because of impaired retinal iron export. Retinal *Hepc1* mRNA levels (Fig. 7A) in DKO mice were increased 3.3-fold compared with the age-matched WT mice ($n = 3$; $P < 0.05$). To determine whether bone morphogenic protein 6 (*BMP6*) or IL-6, which are known to upregulate *Hepc1*,[35,36] might mediate the *Hepc1* increase in DKO retinas, we assessed levels of BMP6 and IL-6 mRNA in DKO versus WT and found no difference ($n = 3$; data not shown). These potential Hepc regulatory pathways may not be responsible for the observed *Hepc* upregulation in the DKOs.

The extracellular carrier protein transferrin (Tf) is abundant in the eye.[37,38] To determine whether *Hepc* can be upregulated by Holo-Tf in the retina, as in hepatocytes,[39] Holo-Tf was introduced into the eye by intravitreal injection. However, in control WT mice, whose eyes were penetrated with the needle without injection of any substance, retinal *IL6* levels were increased (Fig. 7B; $n = 3$). The increased *IL6* resulted in marked *Hepc* upregulation, as needle injury–induced *Hepc* upregulation was abolished in $IL6^{-/-}$ mice (Fig. 7C; $n = 3$).

Thus, to test for Holo-Tf–induced *Hepc* upregulation, it was useful to remove the confounding influence of needle injury–induced *IL6* upregulation. To accomplish this, Holo-Tf was injected into one eye and iron-free transferrin (Apo-Tf) was injected into the other eye of $IL6^{-/-}$ mice. Injection of Holo-Tf caused a 4.5-fold increase in retinal *Hepc* mRNA 8 hours after injection compared with injection of Apo-Tf (Fig. 7D; $n = 3$; $P < 0.05$). Twenty-four hours after Holo-Tf injection, *Hepc* mRNA levels were still elevated twofold (Fig. 7E; $n = 3$; $P < 0.05$). There was no difference in *BMP6* mRNA levels in Holo versus Apo-Tf–injected eyes at 8 hours ($n = 3$; data not shown) or at 45 minutes or 3 hours after injection ($n = 3$; not shown), suggesting that BMP6 was not responsible for the *Hepc* upregulation in this experiment.[35,36]

Mechanisms of Hepc Upregulation in the Mouse Retina

In cultured hepatocytes, Holo-Tf appears to induce Hepc upregulation through the ERK and SMAD pathways.[39] Evidence suggests TfR2 binding to Holo-Tf activates ERK through phosphorylation,[40,41] whereas SMAD1/5/8 activation by phosphorylation can be triggered by BMP6 binding to a complex, including BMP receptor plus hemojuvelin.[42] To test whether Holo-Tf injection activates SMAD1/5/8 and ERK1/2, we assessed levels of the phosphorylated forms of these proteins by Western blot analysis. At 1 hour (Fig. 8) but not at 3 hours (not shown) after injection, the retinal p-ERK/ERK ratio was higher in Holo-Tf– than Apo-Tf–injected retinas. In contrast, p-SMAD levels were similar in Holo-Tf versus Apo-Tf retinas at 1 hour (Fig. 8; $n = 4$) and also at 30 minutes, 3 hours, 5 hours, and 24 hours (not shown), suggesting that the ERK but not the BMP6/SMAD pathway was responsible for the Hepc upregulation in this experiment.

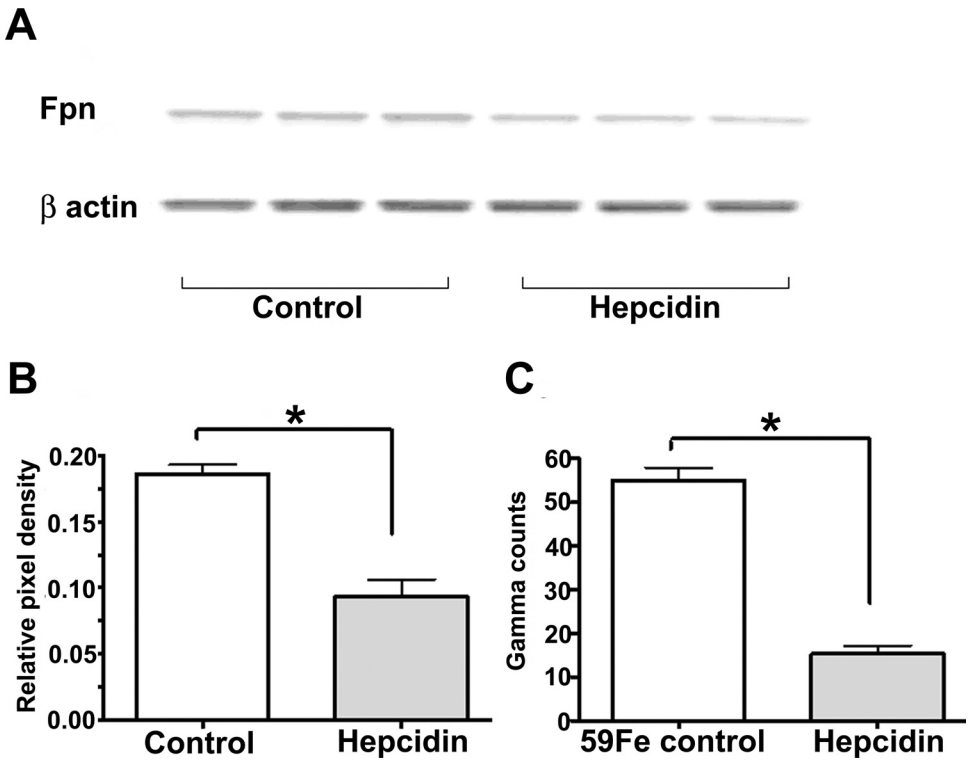

FIGURE 6. Exogenous Hepc peptide decreased Fpn protein levels in BRECs and also reduced iron release from BRECs. Western blot analysis for Fpn (**A**) in BRECs exposed to Hepc peptide for 1 hour and control BRECs not exposed to Hepc, quantified by densitometry and standardized to β-actin (**B**). BRECs exposed to Hepc peptide showed significant decreases (*$P < 0.01$) in the levels of Fpn protein compared with control BRECs. In a separate experiment, a monolayer of BRECs preloaded with 59Fe released significantly less (*$P < 0.001$) 59Fe into the basal chamber (as measured in gamma counts after 1 hour) when Hepc peptide was placed in the basal chamber compared with the no Hepc control condition (**C**).

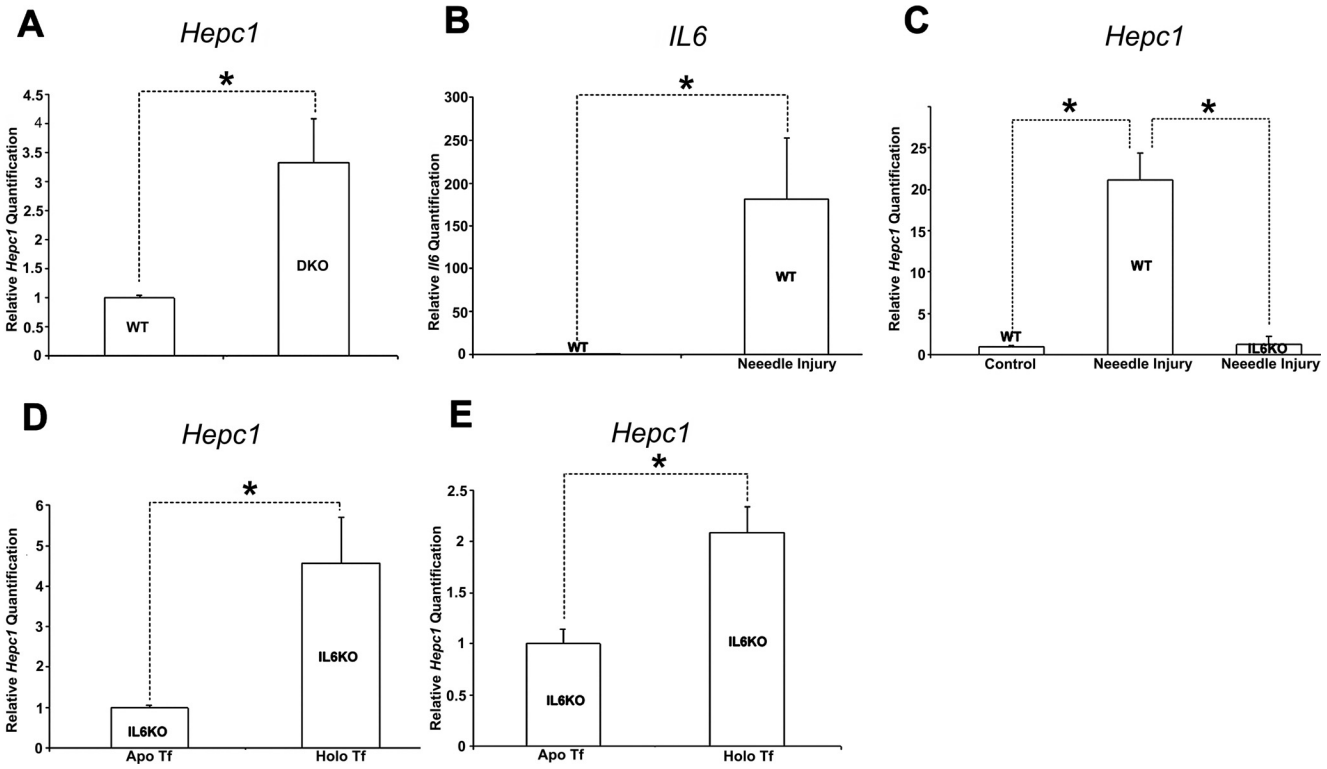

FIGURE 7. *Hepc* mRNA levels in mice with chronic (DKO) or acute (Holo-Tf injection) iron accumulation. *Hepc* mRNA levels measured by qPCR were significantly higher in *Cp/Heph* DKO mice than in age-matched controls (**A**). Needle injury significantly upregulated retinal *IL6* (**B**) and *Hepc* (**C**) mRNA levels in WT but not in $IL6^{-/-}$ (**C**) mice. Retinal *Hepc* mRNA levels were higher in Holo-Tf–injected $IL6^{-/-}$ mice than in control $IL6^{-/-}$ mice injected with Apo-Tf at 8 hours (**D**) and 24 hours (**E**) after injection. $^{*}P < 0.05$.

DISCUSSION

The peptide hormone hepcidin (Hepc) is the master iron regulator; inappropriately low levels contribute to most cases of hereditary hemochromatosis.[43] Herein, we tested whether the retina may produce Hepc to limit retinal iron import, thereby preventing iron toxicity. The absence of Hepc, in $Hepc1^{-/-}$ mice, results in age-dependent retinal iron accumulation (Fig. 3) followed by retinal degeneration (Fig. 1). Levels of the iron transporter ferroportin (Fpn), whose degradation can be triggered by Hepc, are increased in vascular endothelial cells in $Hepc1^{-/-}$ mice (Fig. 5). Conversely, exogenous Hepc decreased Fpn levels in cultured retinal capillary endothelial cells (Figs. 6A, 6B) and decreased iron export from the basal side of the cells (the retina-facing side; Fig.

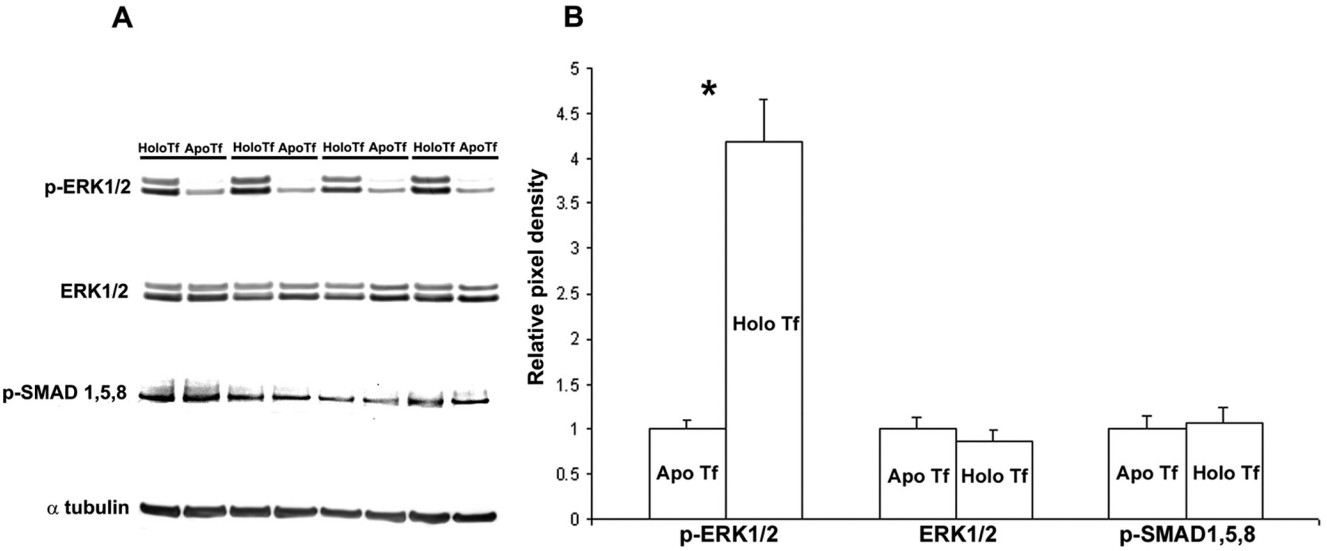

FIGURE 8. Western blot analysis of retinal p-ERK and p-SMAD after intravitreal injection of Holo-Tf. One hour after intravitreal injection of Holo-Tf, p-ERK levels increased compared with control Apo-Tf–injected contralateral eyes. Western blot analysis from four mice (eight retinas) is shown (**A**) and quantified by densitometry (**B**). p-ERK and ERK band intensities were standardized to α-tubulin. p-SMAD levels were unchanged in Holo-Tf compared with Apo-Tf–injected eyes. $^{*}P < 0.05$.

6C). When the retina senses increased iron levels (in *Cp/Heph* DKO mice or after intravitreal iron injection; Fig. 7), it increases Hepc production. Taken together, these results suggest a potential retina-autonomous iron regulatory pathway in which excess retinal iron triggers Hepc upregulation. The Hepc then causes Fpn degradation at the blood-retinal barriers, limiting retinal iron uptake.

Holo-Tf concentration within the eye is substantial,[44,45] and sensing of Holo-Tf concentration appears to be a mechanism of Hepc regulation in hepatocytes. Administration of Holo-Tf to cultured primary cells can upregulate Hepc.[39] In these hepatocytes, Holo-Tf binding to transferrin receptor 2 (TfR2), with resultant phosphorylation of ERK1/2 and SMAD 1/5/8, is thought to trigger increased Hepc transcription.[39] In the retina, the ratio of phospho-ERK1/2 to unphosphorylated ERK1/2 was significantly increased 30 minutes and 1 hour after intravitreal Holo-Tf injection (Fig. 8), suggesting that ERK plays a role in retinal Hepc upregulation induced by Holo-Tf. Yet, the phospho-SMAD/SMAD ratio did not increase at 30 minutes, 1 hour, 3 hours, 5 hours, or 24 hours after Holo-Tf injection. This is consistent with our finding that BMP6 mRNA is not upregulated in *Cp/Heph* DKO– or Holo-Tf–injected retinas, suggesting that the BMP6/SMAD pathway is not responsible for Hepc upregulation in response to elevated neural retinal iron levels in these model systems.

Hepc levels can also be elevated in hepatocytes by inflammation, primarily through IL-6.[46] This mechanism of Hepc regulation also appears to occur in the retina because penetrating needle injury, which increased retinal *IL6* mRNA, also increased retinal *Hepc* mRNA, and the increase in *Hepc* mRNA was abolished in IL-6 knockout mice (Fig. 7). The IL-6–mediated upregulation of Hepc in response to retinal needle injury is consistent with increased retinal *Hepc* mRNA levels seen after intravitreal injection of the proinflammatory molecule lipopolysaccharide.[25] Together, these results suggest that diseases featuring ocular inflammation may cause retinal iron dysregulation.

Consistent with a proposed role for Hepc in limiting retinal iron uptake, *Hepc1*$^{-/-}$ mice had elevated iron levels in the retinal neurons and in the RPE. Although the amount of iron in the neural retina of *Hepc1*$^{-/-}$ mice was below the sensitivity for Perls' staining, increases in neural retinal iron were detectable directly by atomic absorption spectrophotometry (Fig. 3) and indirectly by elevated ferritin protein levels and diminished TfR mRNA levels (Fig. 4). The iron levels in the RPE and ciliary body of *Hepc1*$^{-/-}$ mice reached high enough levels for detection by Perls' staining (Fig. 3).

The elevated neural retina and retinal pigment epithelial iron levels may be exacerbated by the increased serum iron concentration in *Hepc1*$^{-/-}$ mice. It is even possible that iron "leaked" across the blood-retinal barrier because of high serum iron levels independent of any effect of Hepc on local iron regulation. However, chronically elevated serum iron levels caused by a high-iron diet in WT mice do not cause increased mouse retinal iron levels or retinal degeneration (unpublished data). Further evidence that the retina exerts local control over its iron levels comes from *Cp/Heph* DKO mice, in which the retina becomes iron overloaded despite low serum iron levels and anemia.[26,27] Given that Fpn is expressed within the retina not only at the blood-retinal barriers (vascular endothelial cells and retinal pigment epithelial cells) but also within the neural retina in Müller glia and neurons, Hepc dysregulation could affect not only iron transfer into the retina across the blood-retinal barriers but also intercellular iron transfer within the neural retina.

The retinal degeneration in *Hepc1*$^{-/-}$ mice occurs at advanced ages, after retinal iron accumulation. The degeneration consists of photoreceptor death, retinal pigment epithelial hypertrophy with autofluorescence, and rare subretinal neovascularization (Fig. 1). The retinal pigment epithelial autofluorescence spectral analysis suggests that iron-induced oxidative damage results in an accumulation of similar autofluorescent molecules in the *Hepc1*$^{-/-}$ and *Cp/Heph* DKO mice and that some of these are likely present in the RPE in AMD (Fig. 2).

It is surprising that retinal pigment epithelial cells accumulate iron in *Hepc1*$^{-/-}$ mice given that they have elevated Fpn levels that would export more iron from the RPE. It is possible that this retinal pigment epithelial iron results from iron trapping in phagosomes and lysosomes after phagocytosis of iron-laden photoreceptor outer segments. Each retinal pigment epithelial cell normally phagocytoses thousands of outer segment discs per day as part of the photoreceptor renewal process, and these discs are normally high in iron.[47] Ferritin staining in *Hepc1*$^{-/-}$ mice (Fig. 4) indicates that photoreceptor iron levels are even higher than normal in these mice.

Our results suggest several future directions. Hepc is regulated not only by iron but also by inflammation and hypoxia,[22] both of which are associated with AMD.[48–54] Thus, future studies will test whether the dysregulation of retinal Hepc could contribute to iron-exacerbated retinal degeneration in AMD and other retinal diseases. Many patients with hereditary hemochromatosis have inappropriately low levels of Hepc; it will be of interest to determine whether they are at increased risk for retinal or neurodegenerative diseases. Finally, the *Hepc1*$^{-/-}$ mice, in addition to providing new information on regulation of retinal iron homeostasis, provide a model for testing iron chelation for amelioration of retinal degeneration.

Acknowledgments

The authors are grateful for the intellectual and technical contributions of the late John Beard to the study, and they thank Jean-Christophe Deschemin and Xinyu Zhao for technical support.

References

1. Hahn P, Ying GS, Beard J, Dunaief JL. Iron levels in human retina: sex difference and increase with age. *Neuroreport.* 2006;17:1803–1806.
2. Cano M, Thimmalappula R, Fujihara M, et al. Cigarette smoking, oxidative stress, the anti-oxidant response through Nrf2 signaling, and age-related macular degeneration. *Vis Res.* 2010;50:652–664.
3. Sullivan JL. Iron in arterial plaque: modifiable risk factor for atherosclerosis. *Biochim Biophys Acta.* 2009;1790:718–723.
4. Weinberg ED. Iron out-of-balance: a risk factor for acute and chronic diseases. *Hemoglobin.* 2008;32:117–122.
5. Zacharski LR, Chow BK, Howes PS, et al. Decreased cancer risk after iron reduction in patients with peripheral arterial disease: results from a randomized trial. *J Natl Cancer Inst.* 2008;100:996–1002.
6. Zecca L, Youdim MB, Riederer P, Connor JR, Crichton RR. Iron, brain ageing and neurodegenerative disorders. *Nat Rev Neurosci.* 2004;5:863–873.
7. Snyder AM, Connor JR. Iron, the substantia nigra and related neurological disorders. *Biochim Biophys Acta.* 2009;1790:606–614.
8. Lee DW, Andersen JK. Iron elevations in the aging Parkinsonian brain: a consequence of impaired iron homeostasis? *J Neurochem.* 2010;112:332–339.
9. Smith MA, Zhu X, Tabaton M, et al. Increased iron and free radical generation in preclinical Alzheimer disease and mild cognitive impairment. *J Alzheimers Dis.* 2010;19:363–372.
10. Dunaief JL. Iron induced oxidative damage as a potential factor in age-related macular degeneration: the Cogan Lecture. *Invest Ophthalmol Vis Sci.* 2006;47:4660–4664.
11. Gitlin JD. *Aceruloplasminemia*. *Pediatr Res.* 1998;44:271–276.
12. Miyajima H, Kono S, Takahashi Y, Sugimoto M. Increased lipid peroxidation and mitochondrial dysfunction in aceruloplasminemia brains. *Blood Cells Mol Dis.* 2002;29:433–438.
13. Dunaief JL, Richa C, Franks EP, et al. Macular degeneration in a patient with aceruloplasminemia, a disease associated with retinal iron overload. *Ophthalmology.* 2005;112:1062–1065.

14. Donoso LA, Kim D, Frost A, Callahan A, Hageman G. The role of inflammation in the pathogenesis of age-related macular degeneration. *Surv Ophthalmol.* 2006;51:137–152.
15. McGeer EG, Klegeris A, McGeer PL. Inflammation, the complement system and the diseases of aging. *Neurobiol Aging.* 2005; 26(suppl 1):94–97.
16. Ambati J, Anand A, Fernandez S, et al. An animal model of age-related macular degeneration in senescent Ccl-2- or Ccr-2-deficient mice. *Nat Med.* 2003;9:1390–1397.
17. Nemeth E, Ganz T. Regulation of iron metabolism by hepcidin. *Annu Rev Nutr.* 2006;26:323–342.
18. Krause A, Neitz S, Magert HJ, et al. LEAP-1, a novel highly disulfide-bonded human peptide, exhibits antimicrobial activity. *FEBS Lett.* 2000;480:147–150.
19. Nemeth E, Tuttle MS, Powelson J, et al. Hepcidin regulates cellular iron efflux by binding to ferroportin and inducing its internalization. *Science.* 2004;306:2090–2093.
20. Nemeth E, Valore EV, Territo M, Schiller G, Lichtenstein A, Ganz T. Hepcidin, a putative mediator of anemia of inflammation, is a type II acute-phase protein. *Blood.* 2003;101:2461–2463.
21. Pigeon C, Ilyin G, Courselaud B, et al. A new mouse liver-specific gene, encoding a protein homologous to human antimicrobial peptide hepcidin, is overexpressed during iron overload. *J Biol Chem.* 2001;276:7811–7819.
22. Nicolas G, Chauvet C, Viatte L, et al. The gene encoding the iron regulatory peptide hepcidin is regulated by anemia, hypoxia, and inflammation. *J Clin Invest.* 2002;110:1037–1044.
23. Lesbordes-Brion JC, Viatte L, Bennoun M, et al. Targeted disruption of the hepcidin 1 gene results in severe hemochromatosis. *Blood.* 2006;108:1402–1405.
24. Nicolas G, Bennoun M, Porteu A, et al. Severe iron deficiency anemia in transgenic mice expressing liver hepcidin. *Proc Natl Acad Sci U S A.* 2002;99:4596–4601.
25. Gnana-Prakasam JP, Martin PM, Mysona BA, Roon P, Smith SB, Ganapathy V. Hepcidin expression in mouse retina and its regulation via lipopolysaccharide/Toll-like receptor-4 pathway independent of Hfe. *Biochem J.* 2008;411:79–88.
26. Hahn P, Qian Y, Dentchev T, et al. Disruption of ceruloplasmin and hephaestin in mice causes retinal iron overload and retinal degeneration with features of age-related macular degeneration. *Proc Natl Acad Sci U S A.* 2004;101:13850–13855.
27. Hadziahmetovic M, Dentchev T, Song Y, et al. Ceruloplasmin/hephaestin knockout mice model morphologic and molecular features of AMD. *Invest Ophthalmol Vis Sci.* 2008;49:2728–2736.
28. Dunaief JL, Dentchev T, Ying G-S, Milam AH. The role of apoptosis in age-related macular degeneration. *Arch Ophthalmol.* 2002;120: 1435–1442.
29. Schmitz-Valckenberg S, Fleckenstein M, Scholl HP, Holz FG. Fundus autofluorescence and progression of age-related macular degeneration. *Surv Ophthalmol.* 2009;54:96–117.
30. Zhou J, Kim SR, Westlund BS, Sparrow JR. Complement activation by bisretinoid constituents of RPE lipofuscin. *Invest Ophthalmol Vis Sci.* 2009;50:1392–1399.
31. Rouault TA, Hentze MW, Caughman SW, Harford JB, Klausner RD. Binding of a cytosolic protein to the iron-responsive element of human ferritin messenger RNA. *Science.* 1988;241:1207–1210.
32. Rouault T, Klausner R. Regulation of iron metabolism in eukaryotes. *Curr Top Cell Regul.* 1997;35:1–19.
33. Muckenthaler MU, Galy B, Hentze MW. Systemic iron homeostasis and the iron-responsive element/ironregulatory protein (IRE/IRP) regulatory network. *Annu Rev Nutr.* 2008;28:197–213.
34. Burdo JR, Antonetti DA, Wolpert EB, Connor JR. Mechanisms and regulation of transferrin and iron transport in a model blood-brain barrier system. *Neuroscience.* 2003;121:883–890.
35. Meynard D, Kautz L, Darnaud V, Canonne-Hergaux F, Coppin H, Roth MP. Lack of the bone morphogenetic protein BMP6 induces massive iron overload. *Nat Genet.* 2009;41:478–481.
36. Andriopoulos B Jr, Corradini E, Xia Y, et al. BMP6 is a key endogenous regulator of hepcidin expression and iron metabolism. *Nat Genet.* 2009;41:482–487.
37. Vazquez-Quinones LE, Garcia-Castineiras S. A comparative study of iron-related metabolic parameters in the eye of three animal species. *P R Health Sci J.* 2007;26:373–383.
38. Laicine EM, Haddad A. Transferrin, one of the major vitreous proteins, is produced within the eye. *Exp Eye Res.* 1994;59:441–445.
39. Ramey G, Deschemin JC, Vaulont S. Cross-talk between the mitogen activated protein kinase and bone morphogenetic protein/hemojuvelin pathways is required for the induction of hepcidin by holotransferrin in primary mouse hepatocytes. *Haematologica.* 2009;94:765–772.
40. Wallace DF, Summerville L, Crampton EM, Frazer DM, Anderson GJ, Subramaniam VN. Combined deletion of Hfe and transferrin receptor 2 in mice leads to marked dysregulation of hepcidin and iron overload. *Hepatology.* 2009;50:1992–2000.
41. Calzolari A, Raggi C, Deaglio S, et al. TfR2 localizes in lipid raft domains and is released in exosomes to activate signal transduction along the MAPK pathway. *J Cell Sci.* 2006;119:4486–4498.
42. Babitt JL, Huang FW, Wrighting DM, et al. Bone morphogenetic protein signaling by hemojuvelin regulates hepcidin expression. *Nat Genet.* 2006;38:531–539.
43. Viatte L, Vaulont S. Hepcidin, the iron watcher. *Biochimie (Paris).* 2009;91:1223–1228.
44. Tripathi RC, Borisuth NS, Tripathi BJ, Gotsis SS. Quantitative and qualitative analyses of transferrin in aqueous humor from patients with primary and secondary glaucomas. *Invest Ophthalmol Vis Sci.* 1992;33:2866–2873.
45. Clausen R, Weller M, Wiedemann P, Heimann K, Hilgers RD, Zilles K. An immunochemical quantitative analysis of the protein pattern in physiologic and pathologic vitreous. *Graefes Arch Clin Exp Ophthalmol.* 1991;229:186–190.
46. Kartikasari AE, Roelofs R, Schaeps RM, et al. Secretion of bioactive hepcidin-25 by liver cells correlates with its gene transcription and points towards synergism between iron and inflammation signaling pathways. *Biochim Biophys Acta.* 2008;1784:2029–2037.
47. Yefimova MG, Jeanny JC, Keller N, et al. Impaired retinal iron homeostasis associated with defective phagocytosis in Royal College of Surgeons rats. *Invest Ophthalmol Vis Sci.* 2002;43:537–545.
48. Edwards AO, Ritter R 3rd, Abel KJ, Manning A, Panhuysen C, Farrer LA. Complement factor H polymorphism and age-related macular degeneration. *Science.* 2005;308:421–424.
49. Klein RJ, Zeiss C, Chew EY, et al. Complement factor H polymorphism in age-related macular degeneration. *Science.* 2005;308: 385–389.
50. Haines JL, Hauser MA, Schmidt S, et al. Complement factor H variant increases the risk of age-related macular degeneration. *Science.* 2005;308:419–421.
51. Kim YH, He S, Kase S, Kitamura M, Ryan SJ, Hinton DR. Regulated secretion of complement factor H by RPE and its role in RPE migration. *Graefes Arch Clin Exp Ophthalmol.* 2009;247:651–659.
52. Grunwald JE, Metelitsina TI, Dupont JC, Ying GS, Maguire MG. Reduced foveolar choroidal blood flow in eyes with increasing AMD severity. *Invest Ophthalmol Vis Sci.* 2005;46:1033–1038.
53. Arjamaa O, Nikinmaa M. Oxygen-dependent diseases in the retina: role of hypoxia-inducible factors. *Exp Eye Res.* 2006;83:473–483.
54. Metelitsina TI, Grunwald JE, DuPont JC, Ying GS, Brucker AJ, Dunaief JL. Foveolar choroidal circulation and choroidal neovascularization in age-related macular degeneration. *Invest Ophthalmol Vis Sci.* 2008;49:358–363.